BJR

Received: 16 October 2013 | Revised: 17 July 2014 | Accepted: 23 July 2014

doi: 10.1259/bjr.20130654

Cite this article as:
Pauwels R, Zhang G, Theodorakou C, Walker A, Bosmans H, Jacobs R, et al; The SEDENTEXCT Project Consortium. Effective radiation dose and eye lens dose in dental cone beam CT: effect of field of view and angle of rotation. Br J Radiol 2014;87:20130654.

FULL PAPER

Effective radiation dose and eye lens dose in dental cone beam CT: effect of field of view and angle of rotation

[1,2]R PAUWELS, MSc, PhD, [3]G ZHANG, MSc, PhD, [4]C THEODORAKOU, MSc, PhD, [4]A WALKER, MSc, FIPEM, [3]H BOSMANS, MSc, PhD, [1]R JACOBS, MSc, PhD, [5]R BOGAERTS, MSc, PhD and [6]K HORNER, PhD, FRCR; The SEDENTEXCT Project Consortium

[1]Oral Imaging Center, OMFS-IMPATH Research Group, Department of Imaging and Pathology, Faculty of Medicine, Catholic University of Leuven, Leuven, Belgium
[2]Department of Radiology, Faculty of Dentistry, Chulalongkorn University, Bangkok, Thailand
[3]Department of Radiology, University Hospitals Leuven, Leuven, Belgium
[4]Christie Medical Physics and Engineering, The Christie Hospital NHS Foundation Trust, Manchester Academic Health Science Centre, Manchester, UK
[5]Department of Experimental Radiotherapy, University Hospitals Leuven, Leuven, Belgium
[6]School of Dentistry, University of Manchester, Manchester Academic Health Sciences Centre, Manchester, UK

Address correspondence to: Dr Ruben Pauwels
E-mail: *pauwelsruben@hotmail.com*

The SEDENTEXCT Project Consortium listing of partners is available on www.sedentexct.eu

Objective: To quantify the effect of field of view (FOV) and angle of rotation on radiation dose in dental cone beam CT (CBCT) and to define a preliminary volume–dose model.
Methods: Organ and effective doses were estimated using 148 thermoluminescent dosemeters placed in an anthropomorphic phantom. Dose measurements were undertaken on a 3D Accuitomo 170 dental CBCT unit (J. Morita, Kyoto, Japan) using six FOVs as well as full-rotation (360°) and half-rotation (180°) protocols.
Results: For the 360° rotation protocols, effective dose ranged between 54 μSv (4 × 4 cm, upper canine) and 303 μSv (17 × 12 cm, maxillofacial). An empirical relationship between FOV dimension and effective dose was derived. The use of a 180° rotation resulted in an average dose reduction of 45% compared with a 360° rotation. Eye lens doses ranged between 95 and 6861 μGy.
Conclusion: Significant dose reduction can be achieved by reducing the FOV size, particularly the FOV height, of CBCT examinations to the actual region of interest. In some cases, a 180° rotation can be preferred, as it has the added value of reducing the scan time. Eye lens doses should be reduced by decreasing the height of the FOV rather than using inferior FOV positioning, as the latter would increase the effective dose considerably.
Advances in knowledge: The effect of the FOV and rotation angle on the effective dose in dental CBCT was quantified. The dominant effect of FOV height was demonstrated. A preliminary model has been proposed, which could be used to predict effective dose as a function of FOV size and position.

Cone beam CT (CBCT) is an imaging modality using a cone- or pyramid-shaped X-ray beam and a two-dimensional (2D) detector array. It is used in various fields of medicine and was introduced into dentistry in 1996. CBCT produces three-dimensional (3D) information on the facial skeleton and teeth and is being used in many of the dental subspecialties, such as implant dentistry, endodontics, orthodontics and maxillofacial surgery.[1]

Whilst radiation doses in dental CBCT are generally lower than those of multislice CT (MSCT) head examinations, they are higher than those of conventional 2D radiographic techniques (intraoral, panoramic and cephalometric radiography); in both cases, there is some degree of overlap.[2–26] One study has shown that low-dose MSCT protocols are acceptable for maxillofacial surgery and oral implant planning.[27] Therefore, it is crucial to investigate all possible strategies for dose reduction in CBCT imaging to ensure that the basic principles of justification and optimization of patient dose are adhered to.[28]

The field of view (FOV) and its position relative to the radiosensitive organs are key factors determining the radiation dose to the patient.[2–18] In addition, some CBCT scanners expose using a full 360° rotation, whilst others use rotation angles between 180° and 220°. Although the

relationship between FOV, organ doses and effective dose has not yet been quantified, a larger FOV will capture more tissue in the primary X-ray beam and increase the scattered radiation dose to the surrounding tissues. A volume–dose model, which predicts patient dose based on the size and position of the FOV, could be a helpful tool in the context of justification and optimization, as it allows for a straightforward comparison between different FOV options.

The aim of this study was to quantify the effect of FOV and angle of rotation on radiation dose in dental CBCT and to define a preliminary volume–dose model.

METHODS AND MATERIALS

Phantom

The Alderson Radiation Therapy (ART) phantom (Radiology Support Devices, Long Beach, CA) representing an average adult male (height, 175 cm; weight, 73.5 kg) was used in this study. The phantom consists of a polymer mould simulating bone, embedded in a soft tissue equivalent material. It is sectioned into 2.5-cm thick slices, which have a grid of holes for inserting dosemeters. For this study, 11 slices were used, comprising the head and neck region down to the sternoclavicular joint level. The bottom slice was included to ensure that scattered radiation, which covers a relatively wide distance in CBCT, could be fully measured. The holes used for dosimetry in this study were filled up using pins with a $3.2 \times 3.2 \times 0.9$ recess at the top end, allowing for the placement of dosemeter chips. Unused holes were filled up using blank pins.

Equipment

The 3D Accuitomo 170 CBCT unit (J. Morita, Kyoto, Japan) was used in this study. The settings available on this unit are given in Table 1. Dose measurements were performed for selected dental protocols (Table 2) using standard clinical exposure parameters for an adult male, *i.e.* 90 kVp, 5 mA, 17.5 s (87.5 mAs), full rotation (360°). The ratio of the reconstructed volume (*i.e.* geometrical volume) between the largest and smallest FOV is approximately 54:1. For the clinically most common FOVs, additional measurements were obtained using a half rotation (180°, 45 mAs) (Table 2) with the tube rotating posteriorly around the patient (Figure 1).

Table 1. Technical specifications of the 3D Accuitomo 170 CBCT (J. Morita, Kyoto, Japan)

Specification	Value
Voltage	60–90 kVp
Tube current	1–8 mA (high-dose mode)
	1–10 mA (standard-dose mode)
Exposure time (360°/180°)	10.5 s/5.4 s (high-speed mode)
	17.5 s/9.0 s (standard-dose mode)
	30.8 s/15.8 s (high-dose mode)
Exposure type	Continuous
Field of view size (cm)	4×4, 6×6, 8×8, 10×5, 10×10, 14×5, 14×10, 17×5 and 17×12
Source-to-isocentre distance	740–840 mm

For the measurements using a 180° rotation, the FOV position of the corresponding 360° measurement was reproduced exactly using the scout view.

To measure the radiation dose for each exposure, thermoluminescent dosemeter (TLD) chips of the type TLD-100 (LiF:Mg, Ti) were used. To convert the TLD read-out signal (in coulombs) to absorbed dose (in gray), the two-step calibration procedure from Loubele et al[4] was followed. Firstly, for each measurement, 20 calibration TLDs were irradiated using a Harshaw TLD™ Model 6600 Plus reader (ThermoFisher Scientific Inc., Waltham, MA) containing a strontium-90 (^{90}Sr) source with a fixed dose rate. Calibration and phantom TLDs were exposed and read out with identical time intervals, ensuring that they were subject to the same amount of signal fading. This first calibration step allowed for the conversion of the phantom TLD read-out values to a generic units (gU) dose. Secondly, a gU-to-gray conversion factor for diagnostic X-rays was determined by calibrating the ^{90}Sr source using the SCANORA® 3D (Soredex, Tuusula, Finland) CBCT at 85 kVp. This second, one-time calibration was performed by using a head-sized cylindrical water phantom, a set of reference TLDs and a small-volume (0.6 cm^3) ion chamber (Farmer FC65-G; IBA Dosimetry, Schwarzenbruck, Germany). The ion chamber was calibrated in an RQR5 diagnostic beam. The total uncertainty from the TLD measurement system has been estimated at 3–4% for the TLD type, reader and calibration procedure used in this study.[4]

Estimation of absorbed dose, effective dose and eye lens dose

As CBCT exposures can show sharp dose gradients in the horizontal and vertical planes,[29] it is essential to estimate the absorbed dose for each organ by spreading out an adequate number of TLDs throughout it. Therefore, 148 TLDs were placed in the recesses between the ART phantom's slices or at the phantom's surface; their distribution is shown in Table 3. An additional 10 TLDs were used to estimate the background dose, which was subtracted from the measured values. Organs in the head and neck region that are included in the effective dose calculation are bone surface, brain, oesophagus, red bone marrow, salivary glands, skin, thyroid and remainder tissues. For the remainder tissues, the extrathoracic region, lymphatic nodes, muscle and oral mucosa were included. The dose to the eye lens was also measured as there is increasing evidence for its high sensitivity for non-stochastic effects at relatively low doses.[30]

The absorbed dose to each organ or tissue (T) was calculated in different ways, depending on the anatomical distribution of the tissue in question. For the brain, salivary glands, thyroid, oral mucosa and extrathoracic region, all of which are found solely in the head and neck region, the absorbed dose could be calculated as the average value for all TLDs used for these organs. For the other tissues, the fraction of the tissue that was covered by the head and neck portion of the ART phantom was estimated. For muscle and lymphatic nodes, an overall fraction of 5% was applied to the average value of all TLDs; for the oesophagus, a fraction of 10% was used.[9] For bone surface, red bone marrow and skin, organ fractions were determined based on the estimated fractions of these tissues in each slice of the ART

Table 2. Selected dental protocols

Field of view size	Position	Full rotation (360°)[a]	Half rotation (180°)[b]
4 × 4 cm	Upper canine	Yes	Yes
	Lower molar	Yes	No
6 × 6 cm	Upper frontal	Yes	Yes
	Lower molar	Yes	Yes
8 × 8 cm	Both jaws[c]	Yes	Yes
10 × 10 cm	Both jaws[c]	Yes	No
14 × 5 cm	Upper jaw	Yes	No
	Lower jaw	Yes	No
17 × 12 cm	Maxillofacial (both jaws and maxillary sinus)	Yes	Yes

[a]90 kVp, 87.5 mAs (5 mA, 17.5 s).
[b]90 kVp, 45 mAs (5 mA, 9 s).
[c]Simultaneous exposure of upper and lower dentoalveolar regions.

phantom,[31] summing up the contribution of each slice to the total absorbed dose using the equation:

$$D_T = \int f_i D_{Ti} \quad (1)$$

where f_i is the fraction of tissue T in slice i, and D_{Ti} is the average absorbed dose of tissue T in slice i.

As the TLDs were calibrated in water, and given the different dose–energy relationships for different tissues, a tissue/water correction was applied for bone surface, brain, eye lens, lymphatic nodes, muscle, red bone marrow, skin and thyroid. For these tissues, the mass energy absorption coefficients from Publication 44 of the International Commission on Radiation Units and Measurements (ICRU) were selected for a beam energy of 50 keV (Table 4).[32] This corresponds to the mean beam energy of the 3D Accuitomo 170 at 90 kVp, which was determined using full Monte Carlo simulation by Zhang et al.[33] For other organs (*i.e.* extrathoracic region, oesophagus, oral mucosa and salivary glands), no specific coefficients were available in ICRU Publication 44.[32] Considering that the correction factors for most soft-tissue organs in Table 4 are close to 1, no correction was applied for these four organs.

Figure 1. Tube movement during half rotation (180°).

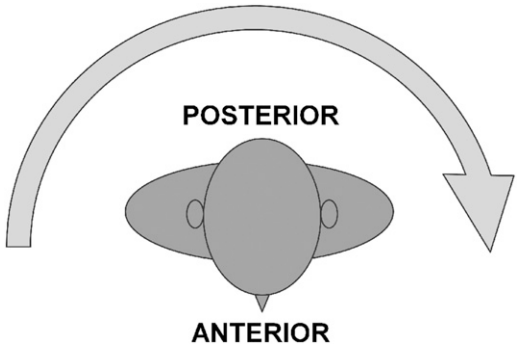

The calculation of the contribution of each organ of interest to the effective dose was performed in two steps. Firstly, the equivalent dose (or radiation weighted dose) to a given organ was determined by multiplying the absorbed dose to that organ by the relevant radiation weighting factor (w_R); w_R expresses the relative biological damage for different types of radiation. Next, equivalent organ doses were multiplied by the tissue weighting factors w_T, which expresses the relative radiation-induced detriment to an organ or tissue. As w_R for X-rays is one, the absorbed dose and equivalent dose are numerically equal. The values of w_T from Publication 103 of the International Commission on Radiological Protection (ICRP) were applied.[34] These are 0.01 for skin, bone surface, brain and salivary glands; 0.04 for thyroid and oesophagus; and 0.12 for red bone marrow and remainder tissues. Only the remainder tissues in the head and neck region were considered, *i.e.* extrathoracic region, lymphatic nodes, muscle and oral mucosa; a dose of 0 μGy was assumed for all other remainder tissues. The effective dose was then calculated as the sum of all organ/tissue contributions.

RESULTS

Table 5 and Figure 2 show the absorbed organ and effective doses for the selected exposure protocols. Effective doses ranged between 54 μSv (4 × 4 cm, upper canine) and 303 μSv (17 × 12 cm, maxillofacial) for full-rotation protocols and between 27 and 169 μSv for half-rotation protocols. The largest absorbed dose was received by the salivary glands, showing a ten-fold range between the lowest and highest absorbed dose (573–5737 μGy). The remainder tissues, salivary glands, red bone marrow and thyroid contributed 90% of the effective dose on average.

An attempt was made to derive an empirical relationship between scanned volume and effective dose, which could be used as a predictive model. The reconstructed volume was defined in two ways. Firstly, as a volume parameter (diameter × height^2), and secondly, as a geometric volume (π × radius^2 × height); diameter and radius refer to the circular dimensions of the FOV along the x- and y-axes (*i.e.* axial plane), and height refers to the

Table 3. Distribution of thermoluminescent dosemeters (TLDs) in Alderson Radiation Therapy phantom (Radiology Support Devices, Long Beach, CA)

Phantom level	Number of TLDs	Organs[a]
0–1	13	BRN
1–2	19	BRN
2–3	22	BRN
3–4	18	BRN, EYE, EXT
4–5	20	SAL, MUC, EXT, LYM
5–6	19	SAL, MUC, EXT, LYM
6–7	17	SAL, MUC, OES, EXT, LYM
7–8	10	SAL, MUC, OES, EXT, LYM
8–9	8	THY, OES, EXT, LYM
9–10	2	THY, LYM

BRN, brain; EXT, extrathoracic region; EYE, eye lens; LYM, lymphatic nodes; MUC, oral mucosa; OES, oesophagus; SAL, salivary glands; THY, thyroid.
Phantom levels refer to the slices between which the TLDs were attached.
[a]Skin, bone surface, red bone marrow and muscle were measured at every level except 9–10.

length of the FOV along the *z*-axis (*i.e.* craniocaudal axis). Using a logarithmic fit, the correlation between the effective dose and FOV dimensions was greater for the volume parameter ($R^2 = 0.97$) than that for the geometric volume ($R^2 = 0.89$) (Figure 3). The use of a quadratic weighting for height for the volume parameter is supported by Table 5, as the effective dose for the 10×10-cm FOV was 46% higher than the average effective dose for the 14×5-cm FOV, although the geometric volumes are similar (*i.e.* 785 and 770 cm^3). The equation of the logarithmic fit using the volume parameter was:

$$E_{NORM} = 0.76 \ln\left(D \times H^2\right) - 2.34 \qquad (2)$$

where E_{NORM} is the tube current exposure time product (mAs)-normalized effective dose (μSv/mAs), and D and H the diameter and height (cm) of the FOV.

Table 4. Correction factors for beam energy

Tissue	Correction factor
Bone surface	5.57
Brain	1.04
Eye lens	0.94
Lymphatic nodes	1.03
Muscle	1.03
Red bone marrow	0.91
Skin	0.96
Thyroid	1.15

Table 5. Organ doses (μGy) and effective doses (μSv) for selected dental protocols

FOV size (cm)[a]	4 × 4		4 × 4	6 × 6		6 × 6		14 × 5	14 × 5	8 × 8		10 × 10	17 × 12	
FOV position	Upper canine		Lower molar	Upper frontal		Lower molar		Upper jaw	Lower jaw	Both jaws		Both jaws	Maxillofacial	
Rotation	Full	Half	Full	Full	Half	Full	Half	Full	Full	Full	Half	Full	Full	Half
Red bone marrow	37	18	69	114	74	94	49	161	124	156	99	295	379	244
Oesophagus	23	14	58	42	26	106	75	73	303	193	103	241	277	129
Thyroid	108	50	236	175	88	433	254	296	813	651	338	799	847	426
Skin	45	27	32	72	50	85	54	108	107	120	70	167	218	130
Bone surface	250	112	178	724	448	305	158	1039	341	682	470	1789	2414	1432
Salivary glands	845	573	2011	2192	1583	3122	2083	3821	3879	4203	2946	5293	5737	3692
Brain	53	21	40	149	116	85	76	210	84	184	112	491	1469	1035
Remainder tissues[b]	273	125	488	492	226	662	349	682	855	887	441	981	950	460
Effective dose	54	27	101	113	62	148	85	168	206	211	118	272	303	169
Eye lens	174	95	146	608	288	255	103	681	203	692	292	5308	6861	2284

FOV, field of view.
[a]Diameter × height of cylindrical reconstructed FOV.
[b]Extrathoracic region, lymphatic nodes, muscle and oral mucosa.

Figure 2. Effective dose (μSv) for selected dental protocols. BJ, both jaws; CBCT, cone beam CT; LJ, lower jaw; LM, lower molar; MF, maxillofacial; UC, upper canine; UF, upper frontal; UJ, upper jaw.

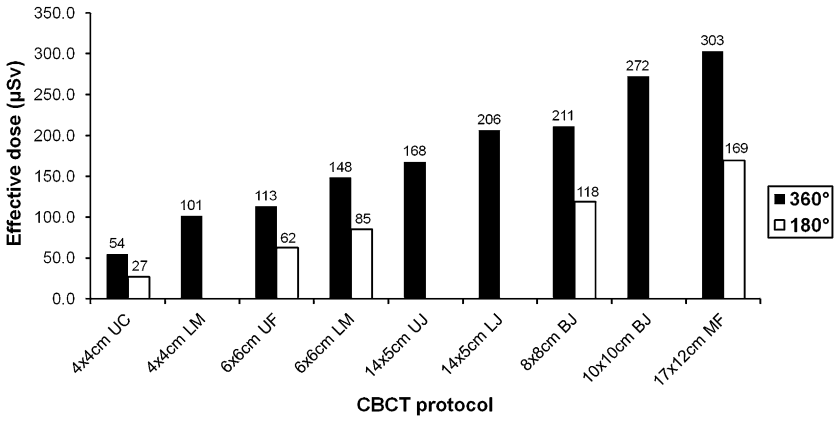

As Equation (2) does not take the position of small-height (<8 cm) FOVs into account, a correction factor was calculated relative to the average value of upper jaw (UJ) and lower jaw (LJ) positions. In this study, UJ and LJ positioning was available only for the 4 × 4, 6 × 6 and 14 × 5 cm FOV. The relative difference between doses for UJ and LJ positioning was the largest for the 4 × 4-cm FOV and the smallest for the 14 × 5-cm FOV. Although the data are limited, there is a clear relationship between dose and FOV (Figure 4). As with the volume–dose model, a logarithmic fit with quadratic weighting for the FOV height was used to quantify the volume dependency of this correction factor. The equations shown in Figure 4 can be rewritten as:

$$CF_{POS} = 1 \pm \left[0.12\ln\left(D \times H^2\right) - 0.80\right] \quad (3)$$

where CF_{POS} is the correction factor for FOV position, D and H the diameter and height of the FOV and ± being positive for maxillary positioning and negative for mandibular positioning. Although Equation (3) does not have a true horizontal asymptote (*i.e.* the two curves in Figure 4 do not converge to $y = 1$), it provides a reasonable estimation of the volume dependency of this correction factor for "realistic" FOV sizes.

The correction factor can be implemented into Equation (2) through basic multiplication, resulting in the following final model:

$$E_{NORM} = CF_{POS} \times \left[0.76\ln\left(D \times H^2\right) - 2.34\right] \quad (4)$$

Comparing 360° and 180° protocols, the average decrease in effective dose was 45% for a half rotation, ranging between 43% for the 6 × 6-cm LJ FOV and 50% for the 4 × 4-cm UJ FOV. The average decrease in absorbed organ dose owing to half rotation ranged between 32% (salivary glands and brain) and 52% (remainder tissues).

Table 5 shows the absorbed doses for the eye lens, which ranged between 95 μGy (4 × 4 cm, upper canine, half rotation) and 6861 μGy (17 × 12 cm, maxillofacial, full rotation). All values are plotted in Figure 5. When compared with the 17 × 12-cm FOV, and with the exception of the 10 × 10-cm FOV, the average reduction in absorbed dose to the eye lens was 93%. The average reduction in eye lens dose between full and half rotation was 56%.

The effect of FOV on dose reduction has also been considered in other studies. Table 6 shows the effect for a 6 × 6 and a 4 × 4 cm

Figure 3. Relationship between normalized effective dose and volume for 360° protocols. For the 4 × 4 cm, 6 × 6 cm and 14 × 5 cm protocols, values for upper jaw and lower jaw positioning were averaged.

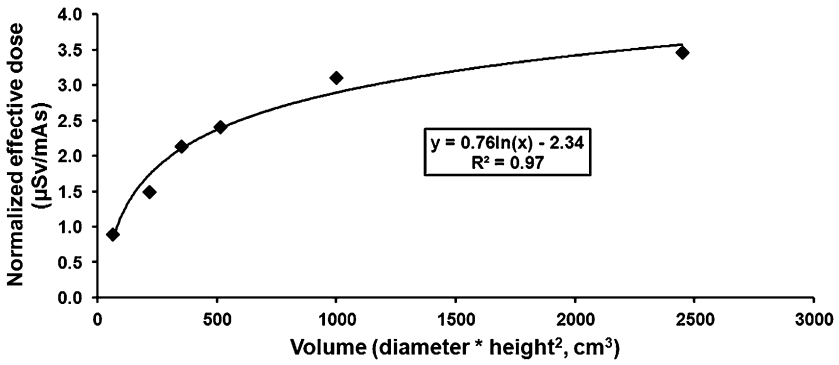

Figure 4. Relationship between correction factors for field of view (FOV) position and volume. Correction factors were calculated as the ratio between the effective dose for upper and lower jaw positioning and the average dose for that FOV.

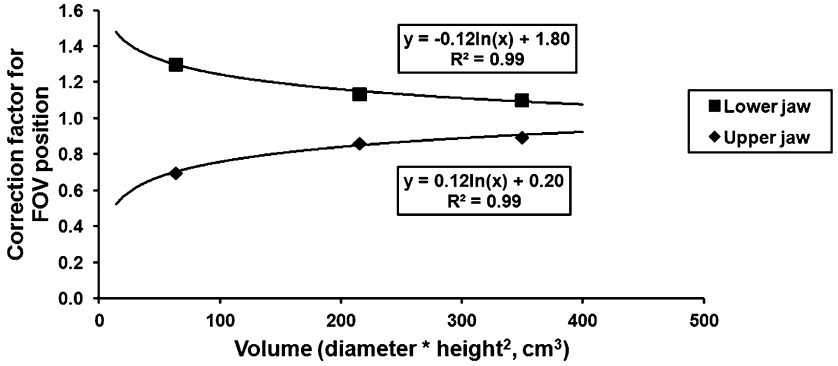

FOV. Table 7 shows the effect for a maxillofacial FOV (*i.e.* 17 × 12 or 16 × 13 cm) and a full-mandible FOV (14 × 5, 16 × 4 or 16 × 6 cm).

DISCUSSION

In this study, the effect of FOV on organ and effective doses in dental CBCT has been quantified for full-rotation (360°) and half-rotation (180°) scanning, and a volume–dose model has been proposed to predict the effective dose (normalized for mAs) as a function of FOV size and FOV position [Equation (4)].

While there have been several published studies showing the effect of FOV on dose, most were limited in the number of FOV options available.[2–18] Although different methodologies may have been used, most studies show a reasonable consistency in the relative dose reduction obtained. Table 7 shows that the use of a 16 × 4-cm FOV covering the mandible compared with a maxillofacial FOV leads to a considerably greater dose reduction (64–69%) than with the use of a 14 × 5- or 16 × 6-cm FOV (26–46%), thus confirming the dominant effect of FOV height. In this study, a 32% dose reduction was seen for the mandibular position of the 14 × 5-cm FOV compared with a 17 × 12-cm FOV. A wide-scale study on 14 dental CBCT models by Pauwels et al[2] demonstrated the overall effect of FOV size and position on organ and effective dose. Loubele et al[4] showed an average reduction of 54% in effective dose for a mandibular MSCT scan (height, 6.0–7.2 cm) compared with a full-head MSCT scan (22.5–22.6 cm). In their paediatric phantom study, Theodorakou et al[18] showed dose reductions of 53% (10-year old) and 40% (adolescent/female) for a mandibular FOV compared with a maxillofacial FOV. It is worth noting that Theodorakou et al[18] included the 3D Accuitomo 170 CBCT scanner in their study, using the 17 × 12-, 14 × 5- and 4 × 4-cm FOVs. However, because of the smaller size of the paediatric phantoms, the effects of changes in FOV size are not directly comparable with the present results. Librizzi et al[7] evaluated the effect of FOV size on dose for temporomandibular joint (TMJ) examinations. Although a dose reduction up to 40% was seen, only large FOV sizes between 15 × 15 cm and 30 × 30 cm were used. Lukat et al[25] measured a dose reduction of ten-fold or more for dual TMJ acquisitions using a small FOV (5.0 × 3.7 cm) compared with a single large-FOV (22.9 × 22.9 cm) exposure, although this reduction does not reflect the pure effect of FOV reduction because the small- and large-FOV measurements were acquired using two different CBCT models with varying exposure parameters.

Although the increase in effective dose owing to the use of a larger FOV is self-evident, the exact relation between FOV and effective dose consists of interplaying factors, *i.e.* FOV height, diameter and position. Based on the current findings, it can be

Figure 5. Absorbed dose to eye lens (μGy) for selected dental protocols. BJ, both jaws; CBCT, cone beam CT; LJ, lower jaw; LM, lower molar; MF, maxillofacial; UC, upper canine; UF, upper frontal; UJ, upper jaw.

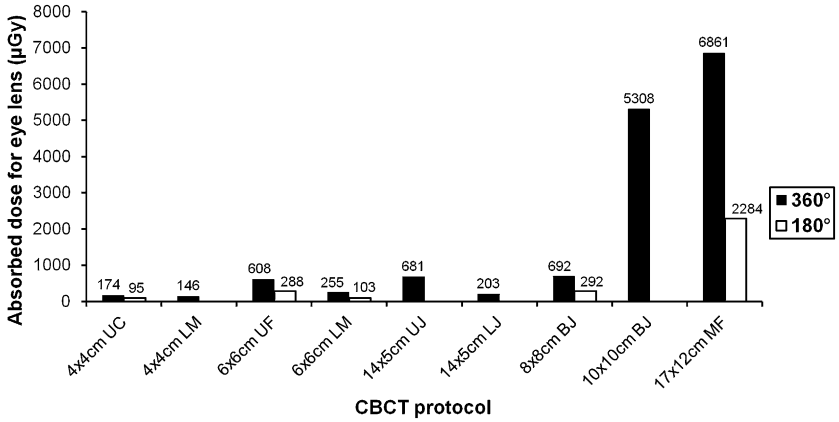

Table 6. Effect of a reduced field of view (FOV) on effective dose (6 × 6 to 4 × 4 cm)

Reference	FOV position	Dose reduction (%)[a]
Current study	Anterior maxilla	52
Hirsch et al[6]	Anterior maxilla	54
Current study	Lower molar	32
Okano et al[3]	Lower molar	51

[a]Relative reduction of the tube current exposure time product-normalized effective dose of a 4 × 4-cm FOV compared with a 6 × 6-cm FOV.

considered that the effective dose will be mainly defined by the height of the FOV and its position. When looking at the results in more detail, it is important to take the relative location of the different organs to the FOV into account. This is clearly shown when comparing mandibular and maxillary positioning of a small-height FOV, or a full head with a single jaw scan. Compared with maxillary scans, mandibular scans result in increased scattered dose to the thyroid. Although mandibular scans decrease the dose to the parotid salivary glands, this is compensated by an increased dose to the submandibular and sublingual salivary glands. Comparing a mandibular scan with a maxillofacial scan, a large increase in effective dose can be expected because of the direct exposure of the parotid salivary glands along with an overall increase in direct and scattered exposure to whole-body organs (*e.g.* bone surface, red bone marrow) and head and neck organs (*e.g.* oral mucosa, extrathoracic region). Increasing the height of the FOV beyond a maxillofacial coverage (*e.g.* >12 cm) will only lead to a marginal increase in effective dose due to the increase in direct exposure to the brain, skin and bone.

This study evaluated the effect of FOV on effective dose and proposed a preliminary volume–dose model that could be used by clinicians and manufacturers to estimate and compare effective doses for different exposure protocols. In addition, this type of model could be adapted to correlate dose indices such as dose–area product or CT dose index to effective dose and aid the determination of diagnostic reference levels.[29] There are a few limitations to the logarithmic fit proposed in this study and its potential use as a predictive model for effective dose in dental CBCT. Firstly, the number of FOVs available for the 3D Accuitomo 170 is limited; the maximum FOV height (12 cm) is smaller than that of certain other CBCT models. Secondly, the correction factor for the position of the FOV was based on only three data points (*i.e.* 4 × 4, 6 × 6, 14 × 5 cm), which limits the applicability of an equation. A logarithmic relation was considered as the most rational choice for this correction factor, but more data points are needed to verify its behaviour. Finally, the relation between FOV size and effective dose may differ between CBCT scanners. In particular, the use of different beam spectra, determined by the kVp value and filtration, leads to varying amounts of beam hardening and scatter. To validate and refine the currently proposed logarithmic volume–dose model, Monte Carlo simulations could be of use, as they would allow selecting and varying exposure parameters beyond the limited set of options available on an actual CBCT device.[16,24,26,33]

Another dose optimization strategy that was assessed in this study is the reduction of the rotation arc, which has the added value of reducing the acquisition time. For the same FOV size and position, a 180° rotation showed a dose reduction of <50%, averaging at 45% when compared with a 360° rotation. On average, the effective dose per mAs increased by 6.7% for 180° protocols compared with corresponding 360° protocols. There is a two-fold explanation for this. First of all, the mAs of the 180° protocol are not exactly half that of the 360° protocol but slightly higher (51.4%). Furthermore, the dose reduction from a 180° rotation is affected by many factors, such as the rotation of the tube (*i.e.* posterior in this study), FOV size and FOV position. For the 4 × 4-cm FOV, the effective dose per mAs was lower for the 180° protocol than that for the 360° protocol. For all other FOV sizes and positions, the effective dose per mAs was slightly higher for the 180° protocol. In a CBCT simulation study by Morant et al,[16] a reduction in effective dose of 40% was calculated for 180° protocols with the tube moving at the posterior side of the head, with an average increase in effective dose per mAs for 180° protocols of 9.5% (based on rounded values). A simulation study by Zhang et al[26] investigated the effect of varying initial positions of the tube for 180° rotations, showing small variations similar to the findings by Morant et al[16] and those of this study. Further investigation is needed to confirm the effect of the starting angle of 180° protocols for a wide range of scanning parameters.

Because of the increasing attention and evidence for deterministic effects (*i.e.* cataract) to the eye lens at low doses, it was included in this study as well. In a recent statement by the ICRP, the threshold for deterministic effects to the eye lens was

Table 7. Effect of a reduced field of view (FOV) on effective dose (maxillofacial to full mandible)

Reference	FOV_1 (cm)	FOV_2 (cm)	Dose reduction (%)[a]
Current study	17 × 12	14 × 5	32
Davies et al[5]	16 × 13	16 × 6	26
Roberts et al[12]	16 × 13	16 × 6	33
Schilling and Geibel[15]	16 × 13	16 × 4	67
Pauwels et al[2]	16 × 13	16 × 6	46
Morant et al[16]	16 × 13	16 × 6	42

[a]Relative reduction of the tube current exposure time product-normalized effective dose of FOV_2 compared with FOV_1.

reduced to 0.5 Gy based on increasing evidence of radiation-induced tissue reactions of the eye lens.[30] Although doses in this study are well below this threshold dose, the ability to decrease eye lens doses through FOV reduction should be kept in mind. An important remark is that the FOV should not be positioned inferiorly to achieve reduction of the eye lens dose, as this could correspond with a severe increase of the thyroid dose. The only acceptable method of dose reduction for the eye lens would be a reduction of the FOV size or any general reduction in exposure (mAs, beam energy).

In conclusion, significant dose reduction can be achieved by reducing the FOV size, particularly the FOV height, of CBCT examinations to the actual region of interest. The proposed volume–dose model can be further refined using additional experimental measurements complemented by Monte Carlo simulations. In addition to FOV reduction, a 180° rotation can be used to further optimize patient dose, as it has the added value of reducing the acquisition time.

FUNDING

The research leading to these results has received funding from the European Atomic Energy Community's Seventh Framework Programme FP7/2007–2011 under grant agreement no. 212246 (SEDENTEXCT: safety and efficacy of a new and emerging dental X-ray modality).

REFERENCES

1. Scarfe WC, Farman AG, Sukovic P. Clinical applications of cone-beam computed tomography in dental practice. *J Can Dent Assoc* 2006; **72**: 75–80.
2. Pauwels R, Beinsberger J, Collaert B, Theodorakou C, Rogers J, Walker A, et al. Effective dose range for dental cone beam computed tomography scanners. *Eur J Radiol* 2012; **81**: 267–71. doi: 10.1016/j.ejrad.2010.11.028
3. Okano T, Harata Y, Sugihara Y, Sakaino R, Tsuchida R, Iwai K, et al. Absorbed and effective doses from cone beam volumetric imaging for implant planning. *Dentomaxillofac Radiol* 2009; **38**: 79–85. doi: 10.1259/dmfr/14769929
4. Loubele M, Bogaerts R, Van Dijck E, Pauwels R, Vanheusden S, Suetens P, et al. Comparison between effective radiation dose of CBCT and MSCT scanners for dentomaxillofacial applications. *Eur J Radiol* 2009; **71**: 461–8. doi: 10.1016/j.ejrad.2008.06.002
5. Davies J, Johnson B, Drage N. Effective doses from cone beam CT investigation of the jaws. *Dentomaxillofac Radiol* 2012; **41**: 30–6. doi: 10.1259/dmfr/30177908
6. Hirsch E, Wolf U, Heinicke F, Silva MA. Dosimetry of the cone beam computed tomography Veraviewepocs 3D compared with the 3D Accuitomo in different fields of view. *Dentomaxillofac Radiol* 2008; **37**: 268–73. doi: 10.1259/dmfr/23424132
7. Librizzi ZT, Tadinada AS, Valiyaparambil JV, Lurie AG, Mallya SM. Cone-beam computed tomography to detect erosions of the temporomandibular joint: effect of field of view and voxel size on diagnostic efficacy and effective dose. *Am J Orthod Dentofacial Orthop* 2011; **140**: e25–30. doi: 10.1016/j.ajodo.2011.03.012
8. Ludlow JB, Ivanovic M. Comparative dosimetry of dental CBCT devices and 64-slice CT for oral and maxillofacial radiology. *Oral Surg Oral Med Oral Pathol Oral Radiol Endod* 2008; **106**: 106–14. doi: 10.1016/j.tripleo.2008.03.018
9. Ludlow JB, Davies-Ludlow LE, Brooks SL, Howerton WB. Dosimetry of 3 CBCT devices for oral and maxillofacial radiology: CB Mercuray, NewTom 3G and i-CAT. *Dentomaxillofac Radiol* 2006; **35**: 219–26. doi: 10.1259/dmfr/14340323
10. Qu XM, Li G, Ludlow JB, Zhang ZY, Ma XC. Effective radiation dose of ProMax 3D cone-beam computerized tomography scanner with different dental protocols. *Oral Surg Oral Med Oral Pathol Oral Radiol Endod* 2010; **110**: 770–6. doi: 10.1016/j.tripleo.2010.06.013
11. Qu X, Li G, Zhang Z, Ma X. Thyroid shields for radiation dose reduction during cone beam computed tomography scanning for different oral and maxillofacial regions. *Eur J Radiol* 2012; **81**: e376–80. doi: 10.1016/j.ejrad.2011.11.048
12. Roberts JA, Drage NA, Davies J, Thomas DW. Effective dose from cone beam CT examinations in dentistry. *Br J Radiol* 2009; **82**: 35–40. doi: 10.1259/bjr/31419627
13. Suomalainen A, Kiljunen T, Käser Y, Peltola J, Kortesniemi M. Dosimetry and image quality of four dental cone beam computed tomography scanners compared with multislice computed tomography scanners. *Dentomaxillofac Radiol* 2009; **38**: 367–78. doi: 10.1259/dmfr/15779208
14. Rottke D, Patzelt S, Poxleitner P, Schulze D. Effective dose span of ten different cone beam CT devices. *Dentomaxillofac Radiol* 2013; **42**: 20120417. doi: 10.1259/dmfr.20120417
15. Schilling R, Geibel MA. Assessment of the effective doses from two dental cone beam CT devices. *Dentomaxillofac Radiol* 2013; **42**: 20120273. doi: 10.1259/dmfr.20120273
16. Morant JJ, Salvadó M, Hernández-Girón I, Casanovas R, Ortega R, Calzado A. Dosimetry of a cone beam CT device for oral and maxillofacial radiology using Monte Carlo techniques and ICRP adult reference computational phantoms. *Dentomaxillofac Radiol* 2013; **42**: 92555893. doi: 10.1259/dmfr/92555893
17. Goren AD, Prins RD, Dauer LT, Quinn B, Al-Najjar A, Faber RD, et al. Effect of leaded glasses and thyroid shielding on cone beam CT radiation dose in an adult female phantom. *Dentomaxillofac Radiol* 2013; **42**: 20120260. doi: 10.1259/dmfr.20120260
18. Theodorakou C, Walker A, Horner K, Pauwels R, Bogaerts R, Jacobs R; SEDENTEXCT Project Consortium. Estimation of paediatric organ and effective doses from dental cone beam CT using anthropomorphic phantoms. *Br J Radiol* 2012; **85**: 153–60. doi: 10.1259/bjr/19389412
19. Chau AC, Fung K. Comparison of radiation dose for implant imaging using conventional spiral tomography, computed tomography, and cone-beam computed tomography. *Oral Surg Oral Med Oral Pathol Oral Radiol Endod* 2009; **107**: 559–65. doi: 10.1016/j.tripleo.2008.11.009
20. Mah JK, Danforth RA, Bumann A, Hatcher D. Radiation absorbed in maxillofacial imaging with a new dental computed tomography device. *Oral Surg Oral Med Oral Pathol Oral Radiol Endod* 2003; **96**: 508–13. doi: 10.1016/S1079210403003500
21. Silva MA, Wolf U, Heinicke F, Bumann A, Visser H, Hirsch E. Cone-beam computed tomography for routine orthodontic treatment planning: a radiation dose evaluation. *Am J Orthod Dentofacial Orthop* 2008; **133**: 640.e1–5. doi: 10.1016/j.ajodo.2007.11.019
22. Tsiklakis K, Donta C, Gavala S, Karayianni K, Kamenopoulou V, Hourdakis CJ. Dose

reduction in maxillofacial imaging using low dose cone beam CT. *Eur J Radiol* 2005; **56**: 413–7. doi: 10.1016/j.ejrad.2005.05.011

23. Jeong DK, Lee SC, Huh KH, Yi WJ, Heo MS, Lee SS, et al. Comparison of effective dose for imaging of mandible between multi-detector CT and cone-beam CT. *Imaging Sci Dent* 2012; **42**: 65–70. doi: 10.5624/isd.2012.42.2.65
24. Koivisto J, Kiljunen T, Tapiovaara M, Wolff J, Kortesniemi M. Assessment of radiation exposure in dental cone-beam computerized tomography with the use of metal-oxide semiconductor field-effect transistor (MOSFET) dosimeters and Monte Carlo simulations. *Oral Surg Oral Med Oral Pathol Oral Radiol* 2012; **114**: 393–400. doi: 10.1016/j.oooo.2012.06.003
25. Lukat TD, Wong JC, Lam EW. Small field of view cone beam CT temporomandibular joint imaging dosimetry. *Dentomaxillofac Radiol* 2013; **42**: 20130082. doi: 10.1259/dmfr.20130082
26. Zhang G, Marshall N, Bogaerts R, Jacobs R, Bosmans H. Monte Carlo modeling for dose assessment in cone beam CT for oral and maxillofacial applications. *Med Phys* 2013; **40**: 072103. doi: 10.1118/1.481967
27. Loubele M, Jacobs R, Maes F, Schutyser F, Debaveye D, Bogaerts R, et al. Radiation dose *vs* image quality for low-dose CT protocols of the head for maxillofacial surgery and oral implant planning. *Radiat Prot Dosimetry* 2005; **117**: 211–16. doi: 10.1093/rpd/nci749
28. Horner K, Islam M, Flygare L, Tsiklakis K, Whaites E. Basic principles for use of dental cone beam computed tomography: consensus guidelines of the European Academy of Dental and Maxillofacial Radiology. *Dentomaxillofac Radiol* 2009; **38**: 187–95. doi: 10.1259/dmfr/74941012
29. Pauwels R, Theodorakou C, Walker A, Bosmans H, Jacobs R, Horner K, et al. Dose distribution for dental cone beam CT and its implication for defining a dose index. *Dentomaxillofac Radiol* 2012; **41**: 583–93. doi: 10.1259/dmfr/20920453
30. Stewart FA, Akleyev AV, Hauer-Jensen M, Hendry JH, Kleiman NJ, Macvittie TJ, et al. ICRP Publication 118: ICRP statement on tissue reactions/early and late effects of radiation in normal tissues and organs—threshold doses for tissue reactions in a radiation protection context. *Ann ICRP* 2012; **41**: 1–322.
31. Huda W, Sandison GA. Estimation of mean organ doses in diagnostic radiology from Rando phantom measurements. *Health Phys* 1984; **47**: 463–7.
32. International Commission on Radiation Units and Measurements. *Tissue substitutes in radiation dosimetry and measurement*. Bethesda, MD: ICRU; 1989.
33. Zhang G, Pauwels R, Marshall N, Shaheen E, Nuyts J, Jacobs R, et al. Development and validation of a hybrid simulation technique for cone beam CT: application to an oral imaging system. *Phys Med Biol* 2011; **56**: 5823–43. doi: 10.1088/0031-9155/56/18/004
34. The 2007 Recommendations of the International Commission on Radiological Protection. ICRP Publication 103. *Ann ICRP* 2007; **37**: 1–332.